Many-body analysis of the effects of electron density and temperature on the intersubband transition in GaAs/$Al_xGa_{1-x}As$ multiple quantum wells

Danhong Huang
Department of Electrical and Computer Engineering, Wayne State University, Detroit, Michigan 48202

Godfrey Gumbs
Department of Physics, Hunter College of City University of New York, 695 Park Ave., New York, New York 10021

M. O. Manasreh
Phillips Laboratory (PL/VTRP), Kirtland Air Force Base, New Mexico 87117
(Received 28 June 1995)

Infrared absorption spectroscopy is used to study conduction electron intersubband transitions between the ground and first excited states in a Si-doped $Al_{0.3}Ga_{0.7}As$/GaAs quantum well. A line-shape calculation is presented for the absorption coefficient as a function of the incident photon energy for different values of T and n_{2D} (where 2D is two dimensional). Good agreement between the numerical results and the experimental data is achieved. The measured blueshift or redshift of the peak position is quantitatively reproduced as T or n_{2D} is reduced, respectively. In the theory, the quasi-particle eigenstates are obtained using a self-consistent Hartree potential and a z-dependent effective mass and nonparabolic energy dispersion. The screened exchange interaction is calculated based on the Hartree self-consistent wave functions and the Thomas-Fermi screening model, and is found to play a crucial role in the T- and n_{2D}-dependence. The many-body theory includes the depolarization shift from a collective dipole moment and the excitonic shift from the vertex correction.

One way of monitoring changes in the material optical response is to use a light probe that perturbs the materials studied. Optical absorption has proven to be one of the simplest and most applicable methods[1–4] to characterize materials. A full understanding of their optical properties will be important because of their potential use as optoelectronic devices such as detectors, modulators, and lasers. The band-structure design of these devices requires a simple but accurate theory for numerical simulations. Early work[5] on intersubband transitions in Si-doped quantum wells (QW's) showed that the exchange energy plays a nontrivial role on the subband structure. Bandara *et al.*[5] explicitly calculated the exchange correction to the Hartree interaction for electrons in a QW for the case with an occupied lowest subband. However, their study was restricted to zero temperature ($T = 0$) and the infinite barrier model. Szmulowicz *et al.*[6] have generalized it to finite T. But there is an overestimation of the blueshift of the peak position as T is reduced at low electron densities n_{2D} (where 2D is two-dimensional). Simple and intuitive attempts to model the T dependence of the absorption peak positions have shown an increase in the transition energy as T is increased, contrary to experimental data.[1,2] As pointed out by Gumbs, Huang, and Loehr[7] the reason for this failure is an inadequate treatment of the many-body effects. However, there is still a 10% difference[7] in the T dependence of the peak energies compared with the measurement.[1,2] In this paper, we improve the agreement between theory and experiment for the peak positions and compare line shapes. For this, we include the nonparabolicity of the energy bands, the exchange energy, the depolarization shift, and the excitonic effect through vertex correction. In Refs. 6, 8, and 9, both the depolarization shift and exchange interaction were included but the vertex correction[10] was neglected in their theories. Another effect not included by these authors concerns the interference of the refractive index with the energy-loss function, which enters the absorption coefficient. This has a significant effect on the peak position and asymmetry of the line shape. The exchange energy calculated in Refs. 6, 8, and 9 is overestimated because the screening of the exchange interaction was neglected and the electrons were confined by two infinite potential walls. The many-body and interference effects are T and n_{2D} dependent since the Coulomb interaction between electrons depends on the subband population, which varies with T and n_{2D}. In this paper, we calculate the absorption spectrum for different T and n_{2D} so that both the peak positions and line shapes can be compared with the experimental measurements.

In our model, we assume a square-well potential $V_{QW}(z)$ with finite barriers for a $Al_{0.3}Ga_{0.7}As$/GaAs QW. The barrier height is $V_0 = 0.57 \times 1.247x$ eV with $x = 0.3$. The Schrödinger equation, determining the wave function $\phi_j(z)$ and eigenvalue E_j, in the self-consistent Hartree approximation is[2,7]

$$\left[-\frac{\hbar^2}{2m_j^*(0)} \frac{d^2}{dz^2} + V_{QW}(z) + V_H(z) \right] \phi_j(z) = E_j \, \phi_j(z) \ , \tag{1}$$

where $j = 1, 2, 3, \ldots$ is the subband index. The non-

parabolic electron energy dispersion in the GaAs material is included through[11]

$$\frac{m_e}{m_W(k)} = 1 + \frac{E}{3}\left(\frac{2}{E_g + \hbar^2k^2/2m_W} + \frac{1}{E_g + \Delta_0 + \hbar^2k^2/2m_W}\right) , \quad (2)$$

which depends on the in-plane wave vector k. Here, m_e is the free electron mass, m_W is the effective mass in the GaAs material, $E_g = 1.5192 - 5.405 \times 10^{-4}\, T^2/(204+T)$ eV is the energy gap, $\Delta_0 = 0.341$ eV is the spin-orbit splitting, and $E_p = 22.71$ eV is related to Kane matrix elements.[11] Because the effective masses in the well and barrier materials are different, we obtain the "average" effective mass in the QW, using first-order perturbation theory,[7,11]

$$\frac{1}{m_j^*(k)} = \frac{P_j}{m_W(k)} + \frac{1-P_j}{m_B} , \quad (3)$$

which depends on j. Here, m_B is the effective mass in the $Al_xGa_{1-x}As$ barrier region, $P_j = \int_{-L/2}^{L/2} dz\ |\phi_j(z)|^2$ is the QW dwelling probability of electrons, and L is the QW width. Using the virtual crystal approximation[2] for $Al_xGa_{1-x}As$, we have $1/m_B = x/m_{AlAs} + (1-x)/m_W$ with $x = 0.3$, where m_{AlAs} is the effective mass in the AlAs material. Classically, every electron in the QW will be acted on by a total Coulomb force from all the other electrons and ionized donors. The quantum-mechanical counterpart of this is the Hartree potential in Eq. (1) and is given by[2,7]

$$V_H(z) = -\frac{2\pi e^2}{\epsilon_s}\int_{-\infty}^{\infty} dz'\ |z-z'|\,[\,n(z') - N_{im}(z')\,] , \quad (4)$$

where $\epsilon_s = 4\pi\epsilon_0\epsilon_b$, ϵ_b is an average background dielectric constant, and the impurity doping profile is

$$N_{im}(z) = N_{im}^{3D}(z) + \sum_n N_{im}^{2D}(n)\ \delta(z - z_n) . \quad (5)$$

In Eq. (5), $N_{im}^{2D}(n)$ is the sheet density of δ doping in the nth layer at $z = z_n$. The electron-density function is

$$n(z) = \frac{1}{\pi}\sum_j \int_0^{\infty} dk\ k\ n_{jk}\ |\phi_j(z)|^2 , \quad (6)$$

where $n_{jk} = (1 + \exp\{[E_j + \hbar^2k^2/2m_j^*(k) - \mu]/k_BT\})^{-1}$ is the jth subband occupation factor in k space and μ is the chemical potential. Charge neutrality leads us to

$$\int_{-\infty}^{\infty} dz\ n(z) = n_{2D} = \int_{-\infty}^{\infty} dz\ N_{im}^{3D}(z) + \sum_n N_{im}^{2D}(n) , \quad (7)$$

and Eq. (7) can be used to determine μ self-consistently.

The first effect of the Coulomb interaction is the renormalization of the electron kinetic energy. From the calculated self-consistent wave functions $\phi_j(z)$ and eigenvalues E_j, we can further include the exchange interaction, which strongly depends on T and n_{2D}. This brings us to the renormalized electron kinetic energy[12]

$$E_{jk} = E_j + \frac{\hbar^2k^2}{2m_j^*(k)} + \sum_{ik'} n_{ik'}\ V_F^{ij}(|\mathbf{k}-\mathbf{k}'|) , \quad (8)$$

where the exchange-interaction matrix is[7,12]

$$V_F^{ij}(|\mathbf{k}-\mathbf{k}'|) = -\left[\frac{2\pi e^2/\epsilon_s}{|\mathbf{k}-\mathbf{k}'| + q_{TF}S_{TF}(|\mathbf{k}-\mathbf{k}'|)}\right] \times \int_{-\infty}^{\infty} dz \int_{-\infty}^{\infty} dz'\ \phi_j(z)\phi_i(z) \times \exp(-|\mathbf{k}-\mathbf{k}'||z-z'|)\ \phi_i(z')\phi_j(z') . \quad (9)$$

As an electron is excited from state i to j at z, there will be another electron simultaneously making a transition from state j to i at z'. Equivalently, there is an exchange between these two indistinguishable electrons in these two positions. Their fermion character produces a negative sign in the exchange interaction. In Eq. (9), the Thomas-Fermi screening length q_{TF}^{-1} is calculated according to[13]

$$q_{TF} = \left(\frac{2e^2}{\epsilon_s\hbar^2}\right)\sum_j m_j^*(0)\frac{d}{du}\left[\frac{1}{\pi}\arctan\left(\frac{\mu - E_j}{\gamma_j}\right)\right] , \quad (10)$$

where γ_j is the inhomogeneous broadening of the jth subband and

$$S_{TF}(|\mathbf{k}-\mathbf{k}'|) = \left(\frac{1}{n_{2D}^2}\right)\int_{-\infty}^{\infty} dz \int_{-\infty}^{\infty} dz' \times \exp(-|\mathbf{k}-\mathbf{k}'|\,|z-z'|)\, n^2(z) \quad (11)$$

is the correction to q_{TF} (Ref. 13) due to the finite-size distribution of electrons in the QW. In our numerical calculations, we have used the phenomenological formula[2,11] for the impurity-scattering broadening γ_j (meV)$= 3.144 + 0.101 \times 10^{-11} n_{2D}(10^{11}\ \text{cm}^{-2}) + 2.55[\exp(\hbar\omega_{ph}/k_BT) - 1]^{-1}$, where the optical phonon frequency is $\hbar\omega_{ph} = 36.7$ meV. The quadratic n_{2D} term[2] in γ_j is neglected since the impurity scattering is only proportional to n_{2D} in the Born approximation.[13] This completes our way of including the effect of the Coulomb interaction in renormalizing the electron kinetic energy. The Hartree interaction can only produce a shift of the subband edge. However, this shift depends weakly on the subband index, temperature, and electron density compared with the shift produced by the exchange interaction. The dominant exchange interaction also gives rise to an additional nonparabolic energy dispersion. The other effects of the Coulomb interaction on the optical response are described below.

When an external z-polarized electromagnetic field is applied, the resulting perturbation in the electron density

distribution will produce an optical response from a normal mode of density fluctuation. In the long-wavelength limit, only vertical transitions need be considered. The absorption coefficient is[14]

$$\beta_{\rm abs}(\omega) = \frac{\omega\sqrt{\epsilon_b}}{cn(\omega)}\ [\rho_{\rm ph}(\omega)+1]\ {\rm Im}\chi(\omega) \tag{12}$$

with the scaled refractive index function

$$n(\omega) = \frac{1}{\sqrt{2}}[1+{\rm Re}\chi(\omega) + \sqrt{\{1+{\rm Re}\chi(\omega)\}^2+\{{\rm Im}\chi(\omega)\}}^{1/2} \tag{13}$$

where $\rho_{\rm ph}(\omega) = [\ \exp(\hbar\omega/k_BT)-1\ ]^{-1}$ is the photon distribution function and $\hbar\omega$ is the incident photon energy. The susceptibility $\chi(\omega)$ is[14]

$$\chi(\omega) = -\frac{2e^2}{\epsilon_s L}\sum_{jj'}\int_0^\infty dk\ k\ \rho_{jj'}(k,\omega)\ F_{j'j}\ . \tag{14}$$

The first-order density-matrix element from linear response theory is[7,14]

$$\rho_{jj'}(k,\omega) = \left[\frac{n_{jk}-n_{j'k}}{\hbar\omega-(E_{j'k}-E_{jk})+i\gamma_{jj'}}\right] \times\Gamma_{jj'}(k,\omega)\ [F_{jj'}+D^c_{jj'}(\omega)]\ , \tag{15}$$

where $D^c_{jj'}(\omega)$ is the collective dipole moment due to the Hartree interaction as a correction to the dipole moment of noninteracting electrons, i.e., $F_{jj'} = \int_{-\infty}^{\infty} dz\ \phi_j(z)\ z\ \phi_{j'}(z)$, and $\Gamma_{jj'}(k,\omega)$ is the vertex correction due to the excitonic interaction.[10]

The second effect of the Coulomb interaction is the vertex correction to the noninteracting electron polarizability. At the same time when an electron is excited to a higher subband, it creates a "hole" state in the initial occupied subband. This will lead to an "excitonic" interaction between the excited electron and the "hole" state. The vertex part $\Gamma_{jj'}(k,\omega)$ in Eq. (15) can be calculated by summing over all the ladder diagrams, which yield the following equation:[14]

$$\Gamma_{jj'}(k',\omega) = 1+\frac{1}{2\pi}\int_0^\infty dk\ k\ V_F^{jj'}(|\mathbf{k}-\mathbf{k}'|) \times\Pi^{(0)}_{jj'}(k,\omega)\Gamma_{jj'}(k,\omega)\ , \tag{16}$$

where the noninteracting electron polarizability for $E_{jk} < E_{j'k}$ is[7,14]

$$\Pi^{(0)}_{jj'}(k,\omega) = (n_{jk}-n_{j'k})\left[\frac{1}{\hbar\omega-(E_{j'k}-E_{jk})+i\gamma_{jj'}} - \frac{1}{\hbar\omega+(E_{j'k}-E_{jk})+i\gamma_{jj'}}\right]\ . \tag{17}$$

Here, $\gamma_{jj'} = (\gamma_j+\gamma_{j'})/2$ is the dephasing rate. In Eq. (16), the small exciton-coupling effect is neglected for low electron density.

The third effect due to the Coulomb interaction is the screening of $D^c_{jj'}(\omega)$. When an electron is excited to a high subband, it induces a density fluctuation in neighboring electrons through the long-range Coulomb force. This will introduce a screening on $D^c_{jj'}(\omega)$. In the random-phase approximation, $D^c_{jj'}(\omega)$ is the solution of the following linear-matrix equation:[7,14]

$$\sum_{j<j'} D^c_{jj'}(\omega)\Bigg[\ \delta_{nj}\delta_{n'j'} - \frac{1}{\pi}\int_0^\infty dk\ k\ \Pi^{(0)}_{jj'}(k,\omega)\ \Gamma_{jj'}(k,\omega)\int_{-\infty}^\infty dz\int_{-\infty}^\infty dz'\ \phi_n(z)\phi_{n'}(z)\left(-\frac{2\pi e^2}{\epsilon_s}|z-z'|\right)\phi_j(z')\phi_{j'}(z')\Bigg]$$

$$= \frac{1}{\pi}\sum_{j<j'}\int_0^\infty k\ dk\ \Pi^{(0)}_{jj'}(k,\omega)\ \Gamma_{jj'}(k,\omega)F_{jj'}\int_{-\infty}^\infty dz\int_{-\infty}^\infty dz'\ \phi_n(z)\phi_{n'}(z)\left(-\frac{2\pi e^2}{\epsilon_s}|z-z'|\right)\phi_j(z')\phi_{j'}(z')\ . \tag{18}$$

We can see that the screening has been included through the dielectric function shown as a coefficient matrix in Eq. (18). The effect due to screening and the vertex correction tends to shift the peak position up and down, respectively. In addition, screening shrinks the peak width but the vertex correction expands it.

In Fig. 1, we present the absorption coefficient $\beta_{\rm abs}(\omega)$ from both our calculated results using Eq. (12) and experimental data (recorded at the Brewster angle using a Fourier transform infrared spectrometer) for two samples at $T = 5$ K. The peak energy increases with n_{2D}. The positive Hartree energy, depending on n_{2D}, shifts both subbands upward, while leaving their separation almost unchanged. The negative exchange energy shifts the first subband down more than the second subband, thereby increasing their separation. For an increased n_{2D}, the exchange energy becomes dominant. Therefore, the peak position moves to the right. In addition, we find that the calculated peak positions coincide well with those from experiment for both the low- and high-density samples. The peak strength of the low-density peak is slightly lower than that observed in the experiment. The line shapes show slight deviations at energies away from the peak energy and a small peak width is

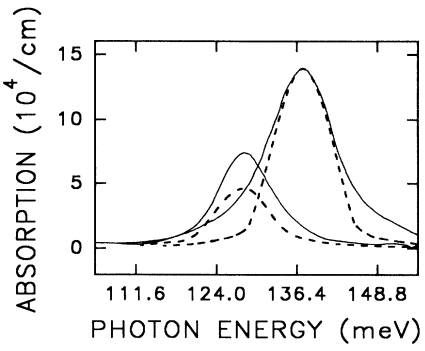

FIG. 1. Comparison between the calculated $\beta_{\rm abs}(\omega)$ (dashed lines) with the measurements (solid lines) at $T = 5$ K for samples with $n_{\rm 2D} = 7.5$ and 37.5×10^{11} cm^{-2}. The high-energy peak is for the high-density sample. In the calculations, the parameters are chosen as $\epsilon_b = 13.0$, $L = 75$ Å, $m_W = 0.0665 m_e$, and $m_{\rm AlAs} = 0.124 m_e$.

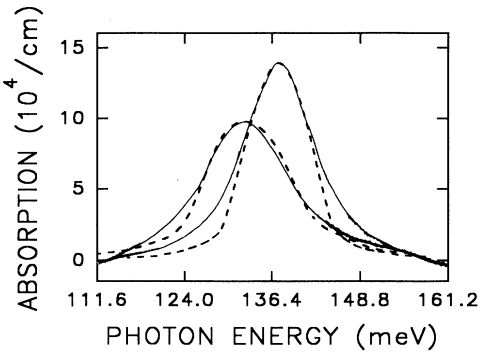

FIG. 3. Comparison between the calculated $\beta_{\rm abs}(\omega)$ (dashed lines) of the sample with $n_{\rm 2D} = 37.5 \times 10^{11}$ cm^{-2} at $T = 5$ K and 300 K with the experimental measurements (solid lines). The high-energy peak is for $T = 5$ K. The chosen parameters for ϵ_b, L, m_W, and $m_{\rm AlAs}$ are the same as in Fig. 1.

obtained in comparison with the measurement. The absorption coefficient $\beta_{\rm abs}(\omega)$ in Eq. (12) contains the ω-dependent refractive index function $n(\omega)$ in the denominator. This produces an interference which changes both the line shape and the peak position. For high $n_{\rm 2D}$, the second subband begins to be populated. The collective dipole moment $D^c_{jj'}(\omega)$ due to the Hartree interaction is found to shrink the peak width, while the exchange interaction expands the peak width. We attribute the asymmetrical line shape to the interference effect, strong nonparabolic energy dispersion at large k, and the exchange interaction.

In Fig. 2 we present a quantitative comparison between $\beta_{\rm abs}(\omega)$ from our numerical simulations and experimental data for the low-density sample at two temperatures. The peak energy increases with reducing T, shown as a blueshift. The crucial negative exchange energy brings down the first subband more than the second subband, and increases the separation between them. With an increase in T, the exchange interaction becomes weaker, and, then, the peak energy decreases. Moreover, we find that the calculated peak positions also coincide with those measured at low and high temperatures. The peak strength of the high-temperature peak seems a bit smaller than that observed. The asymmetrical line shape of both curves displays very small deviations on the lower energy side.

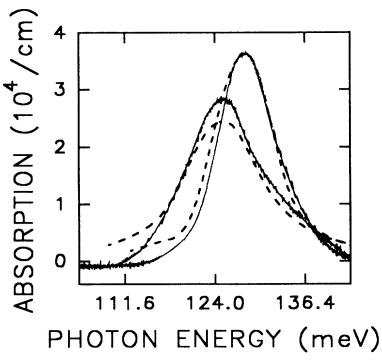

FIG. 2. Comparison between the calculated $\beta_{\rm abs}(\omega)$ (dashed lines) of the sample with $n_{\rm 2D} = 7.5 \times 10^{11}$ cm^{-2} at $T = 5$ K and 300 K with the experimental measurements (solid lines). The high-energy peak is for $T = 5$ K. The chosen parameters for ϵ_b, L, m_W, and $m_{\rm AlAs}$ are the same as in Fig. 1.

Figure 3 shows the numerical comparison between $\beta_{\rm abs}(\omega)$ with the experimental data for the high-density sample at two different temperatures. The peak energy again increases when T is reduced, with a large blueshift compared with Fig. 2 due to high $n_{\rm 2D}$. Similarly, the negative exchange energy lowers the first subband more than the second subband. Therefore, their separation increases with exchange interaction. By reducing T, the exchange interaction is strengthened, so that the peak energy shifts upward. Furthermore, we know that both calculated peak positions and peak strengths for the high-density sample coincide very well with those measured at low and high temperatures. The line shape of both energy peaks, however, differs slightly at energies away from the peak energy. The peak width calculated is smaller than that measured.

In conclusion, by demonstrating reasonably good agreement between our theory and experimental data for absorption from electron intersubband transitions between the ground and first excited states in a $Al_{0.3}Ga_{0.7}As/GaAs$ QW as a function of $n_{\rm 2D}$ and T, we have established a simple but accurate formula for the band-structure design of infrared photodetectors. Our model does not contain any adjustable parameters for comparing the peak positions except for the subband broadening γ_1, γ_2, which are used to fit the full width at half maximum in the experimental data. The blueshift and redshift of the absorption peak position found in the experimental data are quantitatively reproduced theoretically as T and $n_{\rm 2D}$ are reduced, respectively.

[1] M. O. Manasreh, F. Szmulowicz, D. W. Fischer, K. R. Evans, and C. E. Stutz, Appl. Phys. Lett. **57**, 1790 (1990).
[2] M. O. Manasreh and J. P. Loehr, *Semiconductor Quantum Wells and Superlattices for Long Wavelength Infrared Detection* (Artech, Boston, MA, 1993), Chap. 2.
[3] M. O. Manasreh, F. Szmulowicz, T. Vaughan, K. R. Evans, C. E. Stutz, and D. W. Fischer, Phys. Rev. B **43**, 9996 (1991).
[4] P. von Allmen *et al.*, Semicond. Sci. Technol. **3**, 1211 (1988); Superlatt. Microstruct. **5**, 259 (1989).
[5] K. Bandara, D. D. Coon, O. Byungsung, Y. F. Lin, and M. H. Francombe, Appl. Phys. Lett. **53**, 1931 (1988).
[6] F. Szmulowicz, M. O. Manasreh, C. E. Stutz, and T. Vaughan, Phys. Rev. B **50**, 11 618 (1994).
[7] G. Gumbs, D. Huang, and J. P. Loehr, Phys. Rev. B **51**, 4321 (1995).
[8] M. Zaluźny, Solid State Commun. **82**, 565 (1992).
[9] M. Zaluźny, Phys. Rev. B **43**, 4511 (1991).
[10] G. D. Mahan, *Many-Particle Physics* (Plenum, New York, 1981), Chap. 5.
[11] G. Bastard and J. A. Brum, IEEE J. Quantum Electron. **QE-22**, 1625 (1986).
[12] A. H. MacDonald, J. Phys. C **18**, 1003 (1985).
[13] K. Esfarjani, H. R. Glyde, and V. Sa-yakanit, Phys. Rev. B **41**, 1042 (1990).
[14] G. Gumbs, D. Huang, Y. Yin, H. Qiang, D. Yan, F. H. Pollak, and T. F. Noble, Phys. Rev. B **48**, 18 328 (1993).